

# The Mario Schenberg Gravitational Wave Detector: A mathematical model for its quadrupolar oscillations

César A. Costa\* and Odylio D. Aguiar†

*Divisão de Astrofísica, Instituto Nacional de Pesquisas Espaciais  
C.P. 515, São José dos Campos, SP, 122201-907, Brazil*

Nadja S. Magalhães‡

*Instituto Tecnológico de Aeronáutica, Departamento de Física  
Praça Mal. Eduardo Gomes 50,  
São José dos Campos, SP, 12228-900, Brazil*

(Dated: March 29, 2018)

In this work we present a mathematical model for the mechanical response of the Brazilian Mario SCHENBERG gravitational wave (GW) detector to such waves. We found the physical parameters that are involved in this response assuming a linear elastic theory. Adopting this approach we determined the system's resonance frequencies for the case when six  $i$ -mode mechanical resonators are coupled to the antenna surface according to the arrangement suggested by Johnson and Merkwitz: the truncated icosahedron configuration. This configuration presents special symmetries that allow for the derivation of an analytic expression for the mode channels, which can be experimentally monitored and which are directly related to the tensorial components of the GW. Using this model we simulated how the system behaves under a gravitational sinewave quadrupolar force and found the relative amplitudes that result from this excitation. The mechanical resonators made the signal  $\approx 5340$  times stronger. We found  $i + 1$  degenerate triplets plus  $i$  non-degenerate system mode resonances within a band around  $3.17 - 3.24\text{kHz}$  that are sensitive to signals higher than  $\tilde{h} \sim 10^{-22}\text{Hz}^{-1/2}$  when we considerate the effects of thermal noise only.

Keywords: gravitational waves - instrumentation: detectors

## I. INTRODUCTION

The existence of gravitational waves (GWs) was predicted by Einstein applying his General Relativity Theory to the vacuum in the weak field approximation [1]. GWs are local space-time curvature perturbations caused by accelerated masses. These perturbations travel through spacetime with the speed of light and can excite quadrupolar normal-modes of elastic bodies.

Weber was the first one to propose feasible gravitational wave detectors, 43 years ago [2]. However, so far nobody was able to convince the scientific community of any detection. The observable evidence of the existence of these waves comes from an indirect observation in the electromagnetic spectrum of a pulsar radio system [3].

In 1971 Forward suggested the use of a sphere as the antenna element of a resonant-mass detector [4]. He idealized a sphere with nine sets of electromechanical strain transducers placed along great circle routes. The tensor gravitational radiation components would be determined by five independent quantities from the nine transducer outputs. Ashby and Dreitlein studied in detail the reception of GWs by an elastic self-gravitating spherical antenna [5] and Wagoner and Paik found the low-

est eigenvalues for the monopole and quadrupole modes of a uniform elastic sphere [6]. In the 1990's, Johnson and Merkwitz studied the antenna-transducer coupling problem and found an optimum configuration, which minimizes the number of transducers while keeping them in a symmetric distribution on the antenna: the truncated icosahedron (TI) configuration [7]. Magalhaes and collaborators showed that distributions with more resonators also can have interesting symmetric properties [8].

In this work we extend Johnson and Merkwitz's model to two-mode mechanical transducers. This kind of transducer will be used on the **Mario SCHENBERG** spherical detector, which is being constructed in the Physics Institute of the Sao Paulo University with financial support from the State of Sao Paulo Research Foundation (FAPESP).

SCHENBERG has a 65cm-diameter and  $\sim 1150\text{kg}$  copper alloy [Cu(94%)Al(6%)] spherical antenna that will operate at temperatures below 1K. These characteristics are shared with the detectors MiniGrail (The Netherlands) and SFERA (Italy). Figure I shows a schematic diagram of the Schenberg detector.

In this work we consider an isolated sphere coupled only to mechanical resonators and predict the mechanical behavior of the system. We solve the displacement equations of the whole system and find an analytic expression that relates the mode channels measurements to the GWs tensorial components.

---

\*Electronic address: cesar@das.inpe.br

†Electronic address: odylio@das.inpe.br

‡Electronic address: nadjam@ig.com.br

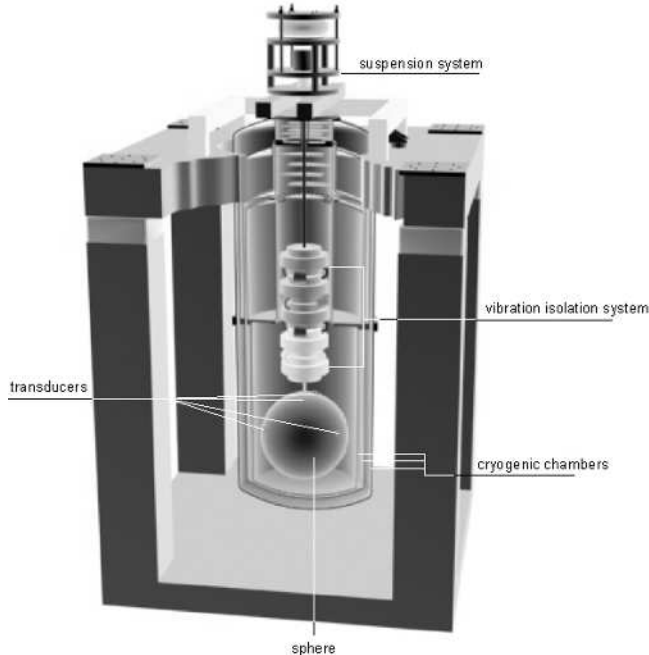


FIG. 1: Schematic diagram of the Brazilian spherical GW detector Schenberg.

## II. THE SPHERE

We will assume that the antenna has a perfect spherical symmetry and ignore the effects caused by the hole machined in the body to attach the suspension rod. We will show in subsection VB by numerical simulations that this is a good approximation for the real case.

Consider a spherical isotropic elastic body with radius  $R$  and density  $\rho$  in a field of forces. The strain suffered by a mass element  $dM$  is described by the displacement vector  $u_i = x'_i - x_i$  (where  $x_i$  represents the equilibrium position and  $x'_i$  denotes the position of  $dM$  after deformation). The strain tensor  $u_{ij}$  is defined by [9]

$$u_{ij} = \frac{1}{2} (u_{i,j} + u_{j,i}), \quad \text{with } i, j = 1, 2, 3. \quad (1)$$

There is a stress tensor  $\sigma_{ij}$  associated to strain tensor by constitutive equations (generalizations of Hooke's law), given by

$$\sigma_{ij} = \delta_{ij} \lambda u_{ll} + 2\mu u_{ij}, \quad (2)$$

where  $\lambda$  and  $\mu$  are Lamé coefficients, which describe elastic properties of a body (they are functions of the Poisson's ratio and the Young modulus). By the application of the principle of conservation of linear momentum we find equilibrium equations given by

$$\sigma_{ij,j} + \rho u_{i,00} = f_i, \quad (3)$$

where  $f_i$  corresponds to the  $i$ -th component of an external force density field and  $\rho u_{i,00}$  to an internal one. These equations are called Navier's equations and can be rewritten by application of equation 2 as

$$(\lambda + \mu)u_{k,ki} + \mu u_{i,jj} + \rho u_{i,00} = f_i, \quad (4)$$

The Navier's equations must be satisfied by a set of functions  $u_i = u_i(x_1, x_2, x_3)$  which represent the displacements inside a region limited by a radius  $R$ . Therefore Equation 4 requires boundary conditions which will indicate that the surface is free to oscillate, defined as

$$n_j \sigma_{ij} = 0, \quad \text{for } r = R, \quad (5)$$

where  $n_i \equiv x_i/r$  is the normal unit.

We assume that it is possible to separate the spacial and temporal dependencies of the displacement vector at a position  $\mathbf{x}$  in a time  $t$ , so we have

$$u_i(\mathbf{x}, t) = \sum_m A_m(t) \Psi_m(\mathbf{x}), \quad (6)$$

where  $A_m(t)$  is the vibrational amplitude of the  $m$ -th normal mode and  $\Psi_m(\mathbf{x})$  is the eigenfunction of this mode. In fact, if the sphere is made of ordinary matter ( $v_{\text{sound}} \ll c$ ) its radius is much smaller than the wavelength and its mechanical quality factor is high ( $Q_m = \omega_m \tau_m \gg 1$ , where  $\omega_m$  and  $\tau_m$  are the angular frequency and the energy time decay of  $m$  mode, respectively) such separation can be done.

The eigenfunctions are normalized according to

$$\int_V \Psi_n(\mathbf{x}) \cdot \Psi_m(\mathbf{x}) d^3x = N_m \delta_{mn}, \quad (7)$$

where  $N_m$  is a arbitrary normalization factor for mode  $m$ . If sphere is homogeneous (with constant  $\rho$ ), we obtain

$$N_m \equiv \frac{4\pi}{3} R^3, \quad \forall m. \quad (8)$$

The equation of motion for the sphere as a forced harmonic oscillator can be obtained from Navier's equation and it is given by

$$\ddot{A}_m(t) + \tau_m^{-1} \dot{A}_m(t) + \omega_0^2 A_m(t) = \frac{1}{\rho N_m} \times \int_{V_0} \Psi_m(\mathbf{x}) \cdot \sum \mathbf{f}(\mathbf{x}, t) d^3x. \quad (9)$$

The eigenfunctions  $\Psi_m(\mathbf{x})$  lead information about the sphere's elastic properties ( $\lambda$  and  $\mu$ ), as well vibrational features (i.g.  $\omega_0$ ).

Specific solutions for Equation 9 can be obtained using spheroidal modes described as linear combinations of the quadrupolar spherical harmonics  $Y_m(\theta, \phi)$  to determine  $\Psi_m(\mathbf{x})$ , which assumes the form [10]

$$\Psi_m(r, \theta, \phi) = [\alpha(r)\hat{\mathbf{r}} + \beta(r)R\nabla]Y_m(\theta, \phi), \quad (10)$$

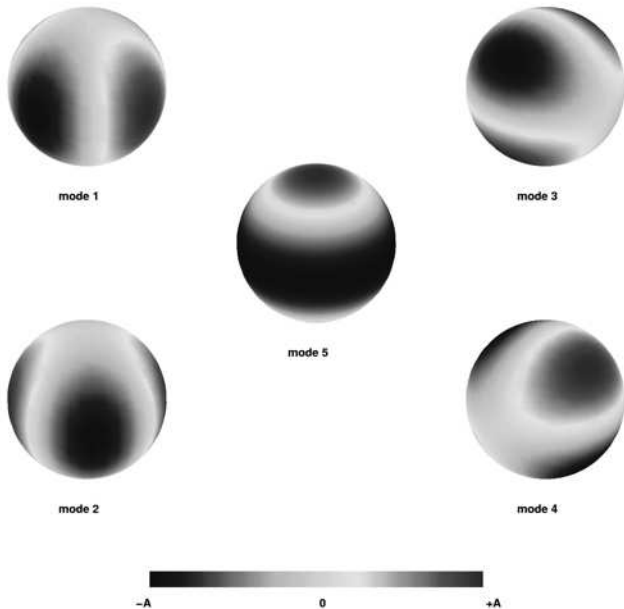


FIG. 2: Quadrupolar normal modes of sphere. The darkest areas represent places of highest radial motion.

where  $\alpha(r)$  and  $\beta(r)$  are respectively the radial and tangential motion parameters. Figure 2 shows the distribution of the radial part of  $\Psi_m$  on the sphere surface, the darkest regions representing the highest radial amplitudes. Ashby and Dreitlein described  $\alpha(r)$  and  $\beta(r)$  function as [5]

$$\alpha(r) = p_1 R \frac{\partial}{\partial r} j_2(qr) + 6p_2 \frac{R}{r} j_2(kr) \quad \text{and} \quad (11)$$

$$\beta(r) = p_1 j_2(qr) + 6p_2 \frac{\partial}{\partial r} [r j_2(kr)], \quad (12)$$

where  $j_2(x)$  is the spherical second order Bessel's function defined as [11]

$$j_2(x) = \left( \frac{3}{x^3} - \frac{1}{x} \right) \sin x - \frac{3 \cos x}{x^2}, \quad (13)$$

and  $q^2 = \rho \omega_0^2 / (\lambda + 2\mu)$  and  $k^2 = \rho \omega_0^2 / \mu$  are respectively the squared transverse and longitudinal wave vectors. The value of the eigenfrequency  $\omega_0$  is determined from Equation 5 which can be rewritten as

$$p_1 \frac{d}{dr} \left[ \frac{j_2(qr)}{r} \right] + p_2 \left[ \frac{10 - (kr)^2}{2r^2} - \frac{1}{r} \frac{d}{dr} \right] j_2(kr) = 0,$$

$$p_1 \left[ \frac{12 - (kr)^2}{2r^2} - \frac{2}{r} \frac{d}{dr} \right] j_2(qr) + 6p_2 \frac{d}{dr} \left[ \frac{j_2(kr)}{r} \right] = 0,$$

where we consider only quadrupolar modes. The values of the normalization parameters  $p_1$  and  $p_2$  are found from the normalization condition given by Equation 7.

Since we know the values of these parameters an expression for effective gravitational force that acts on the

TABLE I: Parameters for the SCHENBERG detector: introduced(1) and obtained from the present model(2).

Description	Symbol	Value
(1) sphere radius at 4K	$R$	0.3239m
(1) sphere mass	$m_S$	1147.85kg
(1) sphere effective mass	$m_{eff}$	287.63kg
(1) mass of resonator $R_1$	$m_{R_1}$	$10^{-5}$ kg
(1) mass of resonator $R_2$	$m_{R_2}$	0.054kg
(1) density at 4K	$\rho$	8065.7kg/m <sup>3</sup>
(1) Young modulus at 4K	$E$	$1.33 \times 10^{11}$ Pa
(1) Poisson's ratio	$\nu$	0.364
(1) linear contraction coefficient <sup>a</sup>	$\Delta R/R$	$334.52 \times 10^{-5}$
(1) bulk Lamè's coefficient at 4K	$\mu$	$4.8753 \times 10^{10}$ Pa
(1) shear Lamè's coefficient at 4K	$\lambda$	$1.3049 \times 10^{11}$ Pa
(1) sphere Q <sup>b</sup>	$Q_S$	$2.0 \times 10^6$
(1) first resonator Q	$Q_{R_1}$	$10^6$
(1) second resonator Q	$Q_{R_2}$	$10^6$
(2) degenerate mode frequencies	$f_0$	3206.3Hz
(2) normalization parameter 1	$p_1$	-5.5654
(2) normalization parameter 2	$p_2$	2.2758
(2) radial parameter at $r = R$	$\alpha(R)$	2.8623
(2) tangential parameter at $r = R$	$\beta(R)$	0.6598
(2) Chi factor	$\chi$	0.6013

<sup>a</sup>Tenderized mean (94%Cu + 6%Al) from [14].

<sup>b</sup>Mechanical quality factor

sphere can be found as

$$\mathcal{F}_m(t) = \frac{1}{2} \ddot{h}_m(t) m_S \chi R, \quad (14)$$

where

$$\chi = \sqrt{\frac{3}{15\pi}} [p_1 j_2(qR) + 3p_2 j_2(kR)] \quad (15)$$

is a factor that determine the effective mass of the sphere, given by [12]

$$m_{eff} = \frac{5}{12} \chi \left( \frac{4\pi}{3} R^3 \right) \rho \Rightarrow m_{eff} \sim \frac{m_S}{4}, \quad (16)$$

and  $h_m = h_m(h_+(t), h_\times(t), \theta, \varphi)$  denotes the spherical amplitude of gravitational wave that depends on the polarization amplitudes and the orientation  $[\theta, \varphi]$  relative to the lab coordinate system centered in the sphere's center of mass (SCM) [13].

We solved the mathematical model for the sphere and found the specific physical parameters of the SCHENBERG detector, as is shown in Table I. The physical dependencies between parameters can be seen in Figures 3, 4 and 5. It is easy to notice that  $\alpha(R)$  and  $\chi(R)$  have small dependence on the Poisson's ratio. Our tests shown that they are practically Young modulus independent. These features imply that little discrepancies on values used in our model will not affect hardly the results obtained in this work.

Evidently, the gravitational force presented in Equation 14 is not the only force that acts on the sphere. The

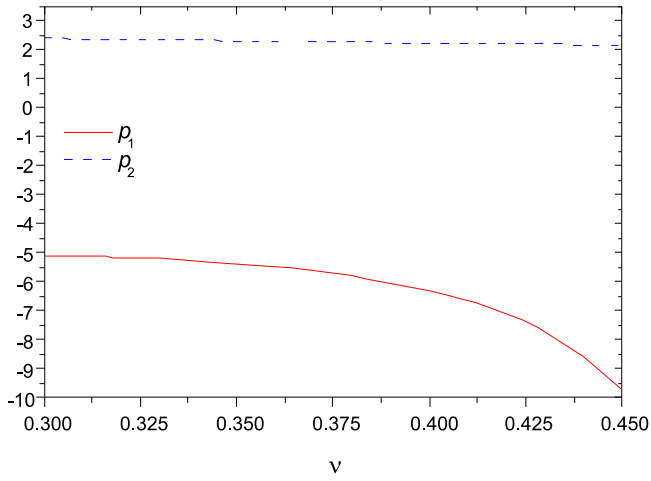


FIG. 3: The normalization parameters dependencies on the Poisson's ratio  $\nu$ .

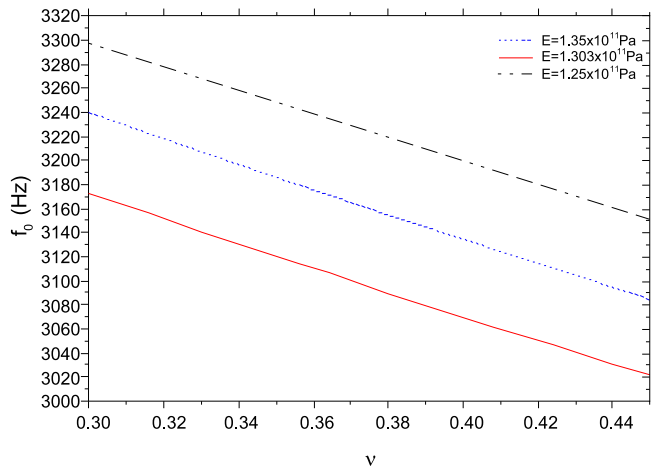


FIG. 4: The resonance frequency  $f_0$  dependence on  $\nu$  and on the Young modulus  $E$ .

resultant force has other components  $F_S^N$  that come from noise sources (e.g. Langevin's forces). These forces must be taken into consideration because they will contribute to the sum of the forces in Equation 9. Thus the sphere will be under the action of the forces  $F_m^S = \mathcal{F}_m + F_S^N$ . Many ways to minimize the noise forces contributions have been studied and a lot of what have been learned in the last decades with bar instruments has been reused and reorganized to be applied to spherical detectors (e.g. vibration isolation systems, cryogenic devices, electromagnetic isolation, etc).

On the other hand, an isolated sphere is not a practical detector since the deformation it suffers due to the GW influence is too small to be detected. Something is needed to work as a impedance transformer. Thus we coupled secondary resonators to the antenna in order to amplify the signal.

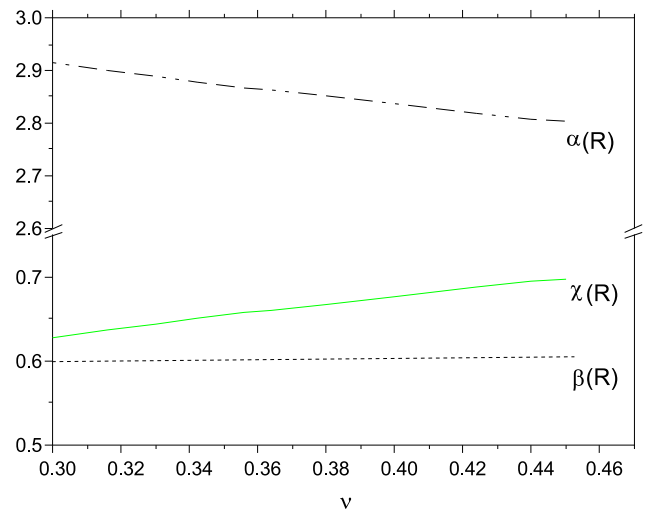


FIG. 5: The radial  $\alpha(R)$  and tangential  $\beta(R)$  displacement parameters and  $\chi(R)$  factor dependencies on  $\nu$  at the sphere surface ( $r = R$ ).

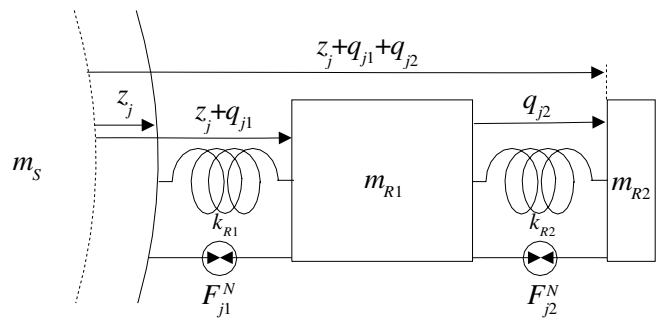


FIG. 6: Unidimensional mechanical resonator with 2 modes attached to the sphere's surface.

### III. THE SPHERE COUPLED TO RESONATORS

Suppose there are  $j$  resonators with 2 modes coupled to the sphere's surface, as it is shown in Figure 6. The resonator is assumed to displace only in the radial direction. When the sphere's surface suffers a radial displacement described by the vector  $z_j$  under each resonator  $j$ , with masses  $m_{R1}$  and  $m_{R2}$  that will represent them henceforth, we have

$$z_j(t) = \hat{\mathbf{r}}_j \cdot \sum_m A_m(t) \Psi_m(t), \quad (17)$$

relative to the SCM, with  $\hat{\mathbf{r}}_j$  being the unit radial vector at the  $j$ -th resonator's position. Thus momentum is transferred to the  $j$  resonator, making  $m_{R1}$  displace  $q_{j1} + z_j$  from the SCM. Thus  $m_{R2}$  moves a distance  $q_{j2} + q_{j1} + z_j$  from that point.

The radial displacements of the sphere's surface under each resonator correspondent to each mode  $m$  can be collected in  $m$  vectors that describe the pattern of the

radial displacement for each mode. Those “pattern vectors” can be grouped in a “pattern matrix”  $B_{mj}$ , defined by [10]

$$B_{mj} = \frac{1}{\alpha} \hat{\mathbf{r}}_j \cdot \Psi_m(x_j), \quad (18)$$

where  $\alpha = \alpha(R)$  represents the radial displacement parameter value at the sphere’s surface. Using Equation 10 we can rewrite 18 as

$$B_{mj} \equiv Y_m(\theta_j, \phi_j). \quad (19)$$

In other words,  $B_{mj}$  represents a spherical harmonic  $Y_m$  behavior at  $x_j$  position  $x_j$ .

The equations of motion of the system can be written in matrix form as

$$\begin{aligned} & \begin{pmatrix} m_S \underline{\underline{I}} & \underline{\underline{0}} & \underline{\underline{0}} \\ m_{R_1} \alpha \underline{\underline{B}}^T & m_{R_1} \underline{\underline{I}} & \underline{\underline{0}} \\ m_{R_2} \alpha \underline{\underline{B}}^T & m_{R_2} \underline{\underline{I}} & m_{R_2} \underline{\underline{I}} \end{pmatrix} \begin{pmatrix} \underline{\underline{\ddot{A}}}(t) \\ \underline{\underline{\dot{q}}}_1(t) \\ \underline{\underline{\dot{q}}}_2(t) \end{pmatrix} + \\ \omega_0^2 & \begin{pmatrix} m_S \underline{\underline{I}} & -m_{R_1} \alpha \underline{\underline{B}} & \underline{\underline{0}} \\ \underline{\underline{0}} & m_{R_1} \underline{\underline{I}} & -m_{R_2} \underline{\underline{I}} \\ \underline{\underline{0}} & \underline{\underline{0}} & m_{R_2} \underline{\underline{I}} \end{pmatrix} \begin{pmatrix} \underline{\underline{A}}(t) \\ \underline{\underline{q}}_1(t) \\ \underline{\underline{q}}_2(t) \end{pmatrix} = \\ & \begin{pmatrix} \underline{\underline{I}} & -\alpha \underline{\underline{B}} & \underline{\underline{0}} \\ \underline{\underline{0}} & \underline{\underline{I}} & -\underline{\underline{I}} \\ \underline{\underline{0}} & \underline{\underline{0}} & \underline{\underline{I}} \end{pmatrix} \begin{pmatrix} \underline{\underline{F}}_S(t) \\ \underline{\underline{F}}_1^N(t) \\ \underline{\underline{F}}_2^N(t) \end{pmatrix}, \quad (20) \end{aligned}$$

where elements double underscored are matrices and single underscored ones are column vectors. We have  $\underline{\underline{B}}^T = [B_{jm}]$  as transpose of  $\underline{\underline{B}} = [B_{mj}]$ ,  $\underline{\underline{I}}$  is the identity matrix and  $\underline{\underline{0}}$  is the null matrix. The dimensions of these matrices depends only of the values of  $j$  and  $m$ .

Equation 20 was obtained assuming that the components of the system have high mechanical quality factor ( $Q > 10^6$ ). Consequently, the damping coefficients are negligible and the time decay of the oscillations tends to infinity.

#### IV. THE RESONATORS’ LOCATIONS

Johnson and Merkowitz suggested that six resonator should be positioned in the center of the pentagonal faces of a truncated icosahedron (TI) concentric to the sphere [7]. The TI configuration has several special symmetries. The pattern matrix can be constructed in such a way that its pattern vectors will be orthogonal in pairs. It has the following properties [10]

$$\underline{\underline{B}} \underline{\underline{B}}^T = \frac{3}{2\pi} \underline{\underline{I}} \quad (21)$$

$$\underline{\underline{B}} \underline{\underline{1}} = \underline{\underline{0}} \quad (22)$$

and the following one, discovered during development of this work:

$$\underline{\underline{B}}^T \underline{\underline{B}} = \frac{3}{2\pi} \underline{\underline{I}} - \frac{1}{4\pi} \underline{\underline{1}} \quad (23)$$

where  $\underline{\underline{1}}$  and  $\underline{\underline{1}}$  are respectively a vector and a matrix in which all elements are the unity, and  $\underline{\underline{0}}$  represents the null vector.

These properties make the TI configuration a good option to the resonator distribution on the sphere because it minimizes their effects on each other while using a small number of resonators, and make possible to obtain an analytic solution to the equations of motion, as shown in section V.

Also, in TI configuration several resonators are affected by a specific sphere mode. So the sphere modes can be monitored by a linear combination of the six resonators outputs. Johnson and Merkowitz have named these linear combinations as mode channels,  $g_m(t)$ , and we have adapted their definition as

$$\underline{\underline{g}}(t) = \underline{\underline{B}} \underline{\underline{q}}_2(t). \quad (24)$$

They are a direct amplified reading of sphere modes.

#### V. A SOLUTION FOR THE EQUATION OF MOTION AND ITS ANALYTIC EXPRESSION

Equation 20 can be rewritten as

$$\underline{\underline{X}} \underline{\underline{\gamma}} \underline{\underline{\ddot{w}}}(t) + \omega_0^2 \underline{\underline{Y}} \underline{\underline{\gamma}} \underline{\underline{w}}(t) = \underline{\underline{Z}} \underline{\underline{F}}(t), \quad (25)$$

where

$$\underline{\underline{\gamma}} \underline{\underline{w}}(t) \equiv \begin{pmatrix} \frac{1}{\sqrt{m_S}} \underline{\underline{I}} & \underline{\underline{0}} & \underline{\underline{0}} \\ \underline{\underline{0}} & \frac{1}{\sqrt{m_{R_1}}} & \underline{\underline{0}} \\ \underline{\underline{0}} & \underline{\underline{0}} & \frac{1}{\sqrt{m_{R_2}}} \end{pmatrix} \underline{\underline{w}}(t) \equiv \begin{pmatrix} \underline{\underline{A}}(t) \\ \underline{\underline{q}}_1(t) \\ \underline{\underline{q}}_2(t) \end{pmatrix}, \quad (26)$$

and  $\underline{\underline{X}}$ ,  $\underline{\underline{Y}}$  and  $\underline{\underline{Z}}$  are the original matrices from equation 20 following their original positions. In this way we solved the problem in a coordinate system based on center of mass, such  $\underline{\underline{\gamma}}$  is the transformation matrix.

We can normalize the equation 25 by multiplying it to  $(\underline{\underline{X}} \underline{\underline{\gamma}})^{-1}$  through left and it became

$$\underline{\underline{\ddot{w}}}(t) + \omega_0^2 \underline{\underline{M}} \underline{\underline{w}}(t) = \underline{\underline{K}} \underline{\underline{F}}(t), \quad (27)$$

in which  $\underline{\underline{M}} \equiv (\underline{\underline{X}} \underline{\underline{\gamma}})^{-1} \underline{\underline{Y}}$  and  $\underline{\underline{K}} \equiv (\underline{\underline{X}} \underline{\underline{\gamma}})^{-1} \underline{\underline{Z}}$ .

The next step is to obtain an orthogonal form of the equation of motion to separate the  $m + 2j$  harmonic oscillators from each other. That results in an equal number of linear equations and simplify the solution of the problem. We assume that  $\underline{\underline{M}}$  is symmetric (and it really is) and therefore it can be diagonalized by using the relation

$$\underline{\underline{U}}^\dagger \underline{\underline{M}} \underline{\underline{U}} = \underline{\underline{D}}, \quad (28)$$

where  $\underline{\underline{U}}$  and  $\underline{\underline{D}}$  represent respectively the matrix which columns are eigenvectors and the eigenvalues diagonal matrix of  $\underline{\underline{M}}$ .  $\underline{\underline{D}}$  must have positive and real values since frequencies must be real and positive. Thus we impose

that  $\underline{U}$  is Hermitian ( $\underline{U}^\dagger \underline{U} = \underline{I}$ ) which assures  $\underline{M}$  is positively defined and  $\underline{D}$  is positive and real. Therefore we can rewrite 27 as

$$\ddot{\underline{\zeta}}(t) + \omega_0^2 \underline{D} \underline{\zeta}(t) \underline{U}^\dagger \underline{K} \underline{F}(t), \quad (29)$$

where  $\underline{\zeta} = \underline{U}^\dagger \underline{w}$ .

Now we can solve the equation of motion in the frequency domain where equation 29 becomes

$$(-\omega^2 \underline{I} + \omega_0^2 \underline{D}) \underline{\zeta}(\omega) = \underline{U}^\dagger \underline{K} \underline{\tilde{F}}(\omega). \quad (30)$$

Since  $\underline{D}$  and  $\underline{I}$  are diagonal matrices the matrix sum in the parentheses is invertible, implying that there is a matrix  $\underline{\tilde{J}}^{-1}(\omega)$  that is equal to that sum and we have

$$\underline{\zeta}(\omega) = \underline{\tilde{J}}(\omega) \underline{U}^\dagger \underline{K} \underline{\tilde{F}}(\omega). \quad (31)$$

To return to the original coordinates we reverse the transformations:

$$\begin{pmatrix} \underline{\tilde{A}}(\omega) \\ \underline{\tilde{q}}_1(\omega) \\ \underline{\tilde{q}}_2(\omega) \end{pmatrix} = \underline{\gamma} \underline{U} \underline{\zeta}(\omega) = \underline{\gamma} \underline{U} \underline{\tilde{J}}(\omega) \underline{U}^\dagger \underline{K} \underline{\tilde{F}}(\omega), \quad (32)$$

which represents the solution of the equation of motion in the frequency domain.

### A. Eigenvalues and eigenvectors

Looking at equation 32 one can check that a good determination of eigenvalues and eigenvectors of  $\underline{M}$  is essential to solve the problem. Moreover, the expressions must rigorously respect imposed conditions. From numerical results for Schenberg's case we noticed that  $\underline{U}$  can be separated into two distinct groups:

$$\underline{U}_{1\pm} = n_{1\pm} \begin{pmatrix} 0 \\ 1 \\ d_{1\pm} 1 \end{pmatrix} \quad \text{and} \quad (33)$$

$$\underline{U}_k = n_k \begin{pmatrix} \underline{I} \\ c_k \underline{B}^T \\ d_k \underline{B}^T \end{pmatrix}, \quad \text{for } k = 2, 3, 4, \quad (34)$$

where  $\underline{U}_k$  corresponds to three degenerate frequencies and  $\underline{U}_{1\pm}$  to isolated frequencies, as is shown in subsection VB. The notation  $\pm$  denotes eigenvectors which refer to up (+) and down (-) shifting of the frequency from the central degeneracy. The values of the constants  $n_{1\pm}$ ,  $d_{1\pm}$ ,  $n_k$ ,  $c_k$  and  $d_k$  are obtained from Equation 28 where

$$\underline{D} = \begin{pmatrix} \lambda_{1\pm} & 0 \\ 0 & \lambda_k \underline{I} \end{pmatrix}, \quad (35)$$

and they are shown in appendix A. Thus we have

$$\underline{\tilde{J}}(\omega) = \begin{pmatrix} \frac{1}{\omega^2 - \omega_{1\pm}} & 0 \\ 0 & \frac{1}{\omega^2 - \omega_k} \underline{I} \end{pmatrix}, \quad (36)$$

where

$$\omega_{1\pm}^2 = \lambda_{1\pm} \omega_0^2 \quad \text{and} \quad \omega_k^2 = \lambda_k \omega_0^2, \quad (37)$$

correspond to the resonant frequencies of the system.

### B. The coupled mode frequencies

Our tests for many  $i$ -mode identical resonators coupled to the sphere using TI configuration results that eigenfrequencies present  $i + 1$  degenerated quintuplets and  $i$  non-degenerated modes. In Mario Schenberg's case we have three degenerate quintuplets ( $f \sim 3175.6, 3206.4, 3237.2\text{Hz}$ ) and two isolated modes ( $f \sim 3184.5, 3228.3\text{Hz}$ ). Figure VB shows how resonance frequencies change as more transducers are coupled to the antenna. The number on the left corresponds to the number of resonators gradually added following the ordering in Figure VB: the number zero corresponds to the isolated sphere; the number one corresponds to resonator 1 coupled to the sphere; the number two corresponds to resonators 1 and 2 coupled to the sphere and so forth. Dashed lines in the results with zero resonators indicate the frequencies measured of the real sphere at 4.2K.

In Figure VB we present how the resonant frequencies should behave when we consider non-degenerate sphere modes, like those resultant from the measurements performed (the dashed lines we mentioned above). We concluded that there is a negligible effect from the suspension hole on the symmetry proprieties of system so we decided to consider degenerate initial modes as a good approximation.

### C. An analytic expression to the solution of the equation of motion

The special symmetries presented by the TI configuration enable us to find an analytic expression to the solution of the equation of motion [8]. After a lengthy calculation we found an analytic expression for the mode channels, given by

$$\begin{aligned} \underline{\tilde{q}}(\omega) &= \frac{3}{2\pi} \frac{1}{\sqrt{m_{R2}}} \sum_{k=2}^4 \eta_k d_k \lambda_k \underline{\tilde{F}}_S(\omega) \\ &+ \frac{3}{2\pi} \frac{\alpha}{b\sqrt{m_{R2}}} q \sum_{k=2}^4 \eta_k d_k \left( c_k - \frac{b+a}{b} \right) \underline{B} \underline{\tilde{F}}_1^N \\ &+ \frac{3}{2\pi} \frac{\alpha}{b\sqrt{m_{R2}}} \sum_{k=2}^4 \eta_k d_k [c_k + d_k(a + a^{-1})] \underline{B} \underline{\tilde{F}}_2^N, \end{aligned} \quad (38)$$

where

$$q = \left( \frac{1}{b} + \frac{3}{2\pi} b \right),$$

$$a = \sqrt{\frac{m_{R2}}{m_{R1}}},$$

and

$$b = \alpha \sqrt{\frac{m_{R2}}{m_S}}.$$

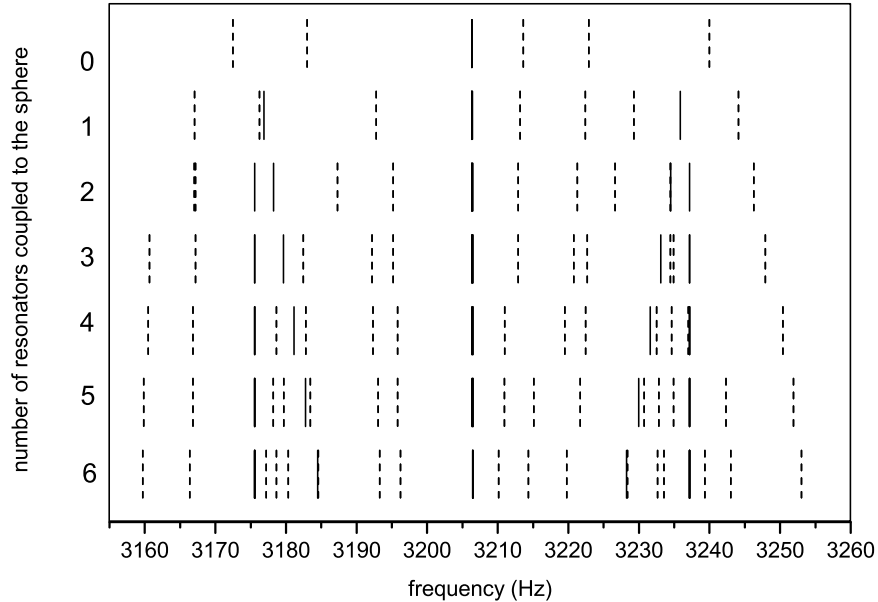


FIG. 7: Frequencies of the coupled modes.

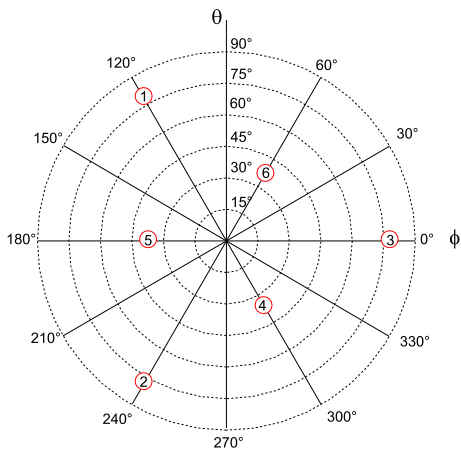


FIG. 8: Projected position of the resonators on the sphere's surface.

The value of  $\eta_k$  depends of  $n_k$ ,  $c_k$  and  $d_k$  values and it also is shown in appendix A.

The above equation results from a combination of equations 24 and 32. It represents the solution of the equation of motion and allows us to know the system's behavior under a gravitational wave excitation.

## VI. NUMERICAL SIMULATION OF THE SYSTEM

In order to test the model we simulated a signal as a gravitational sinewave quadrupolar force with frequency equal to the degenerate normal mode frequencies of the sphere ( $\sim 3206.3\text{Hz}$ ). The signal would be arriving at the local zenith so that its propagation direction coincided with the  $z$  axis of the reference system centered at SCM. Also, we assumed that the simulated gravitational wave had only “ $\times$ ” polarization (“+” polarization was null). Those aspects made only the second normal mode to be excited by the passing of the wave, as shown in Figure 9. We ignored any noise components in this simulation ( $F_i^N = 0$ ).

Special symmetries presented by TI configuration allow only some resonators to oscillate when only the second normal mode is excited, as shown in Figure 10. The number on the right represent relative amplification to maximum amplitude of normal modes of the sphere.

Richard showed (using the Principle of Energy Conservation) that the ratio of displacements [15]

$$\frac{|x_2|}{|x_1|} \equiv \sqrt{\frac{m_1}{m_2}}. \quad (39)$$

We apply this concept to Schenberg's case and found

$$\frac{|q_2|}{|A|} \equiv \sqrt{\frac{m_{eff}}{m_{R_2}}} \simeq 5367, \quad (40)$$

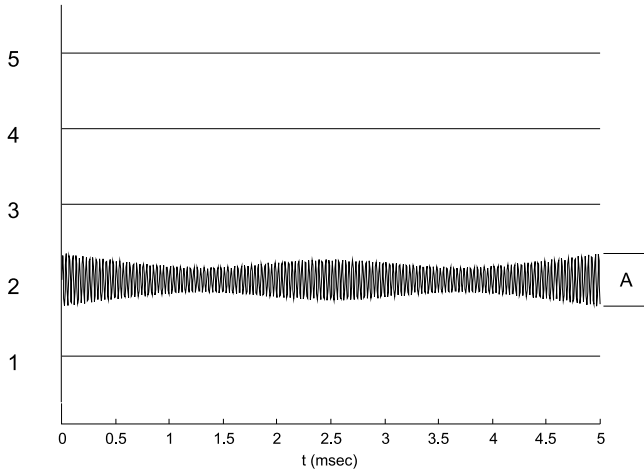


FIG. 9: Responses of the sphere's normal modes to the simulated gravitational wave. Only the second normal mode was excited, as expected.

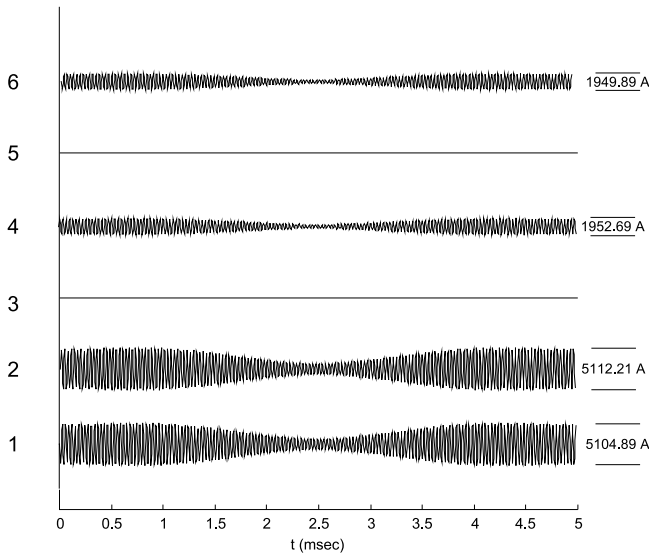


FIG. 10: Amplitudes of the second resonators ( $R_2$ ).

in resonant frequencies. This value is higher than that shown in Figure 10. However as one can observe in Figure 11 no resonator is on a region of maximum amplitude which justifies the difference between the values. Figure 11 presents a plane representation of second normal mode of sphere where darkest areas correspond to maximum displacement loci. One can observe the resonator 3 and 5 are placed on null radial movement areas. Resonators 1 and 2 are placed close of maximum displacement points. An analogous analysis are done for all others normal modes and compatible results are obtained.

From equation 24 we obtain the mode channels outputs as showed in Figure 12.

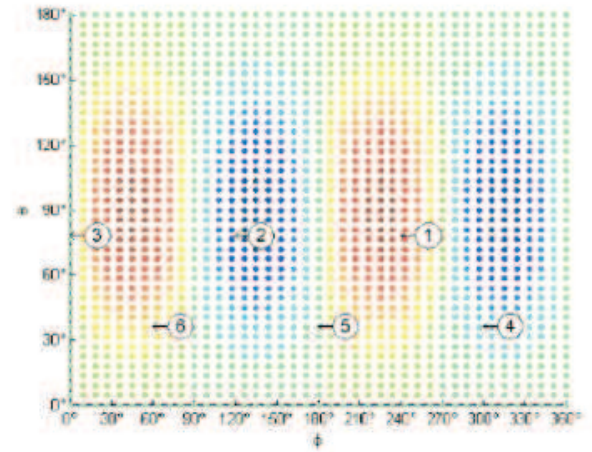


FIG. 11: Location of the transducers compared with second normal mode of the sphere. The darkest areas represent maximum radial amplitude loci.

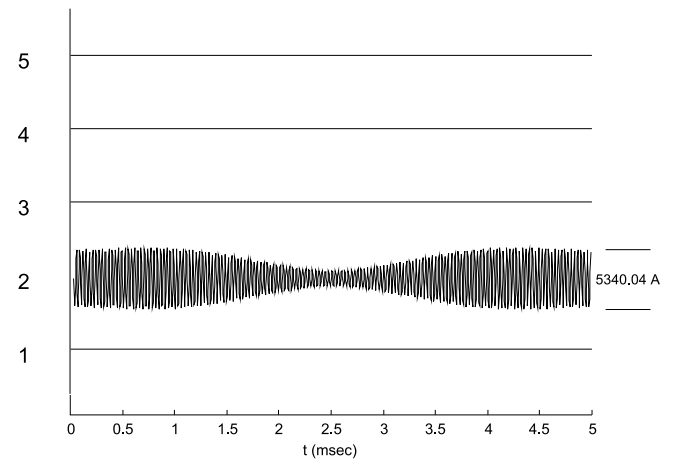


FIG. 12: Mode channel outputs for the simulated signal.

## VII. AN ESTIMATE OF THE NOISE CONTRIBUTION ON THE MODE CHANNELS

We can rewrite Equation 38 as

$$\tilde{g}_m(\omega) = \xi(\omega)\tilde{F}_m^S + \Omega_{mj}^{R_1}(\omega)\tilde{F}_{j1}^N + \Omega_{mj}^{R_2}(\omega)\tilde{F}_{j2}^N \quad (41)$$

where  $\xi(\omega)$  corresponds to the transfer function of the  $\tilde{F}_m^S$  components on  $g_m$ . Similarly, the  $\Omega_{mj}^{R_i}(\omega)$  matrices represent the response functions of mode channel  $m$  to the noise source  $\tilde{F}_{ji}^N$ .

Assuming statistically independent noise sources and ignoring  $\tilde{F}_m$  on  $\tilde{F}_m^S$ , the mode channels spectral densities,  $S_m^g(\omega)$ , can be written as

$$S_m^g(\omega) = |\xi(\omega)|^2 S_{\tilde{F}_m^S} + \sum_j |\Omega_{mj}^{R_1}(\omega)|^2 S_{\tilde{F}_{j1}^N} + \sum_j |\Omega_{mj}^{R_2}(\omega)|^2 S_{\tilde{F}_{j2}^N}, \quad (42)$$



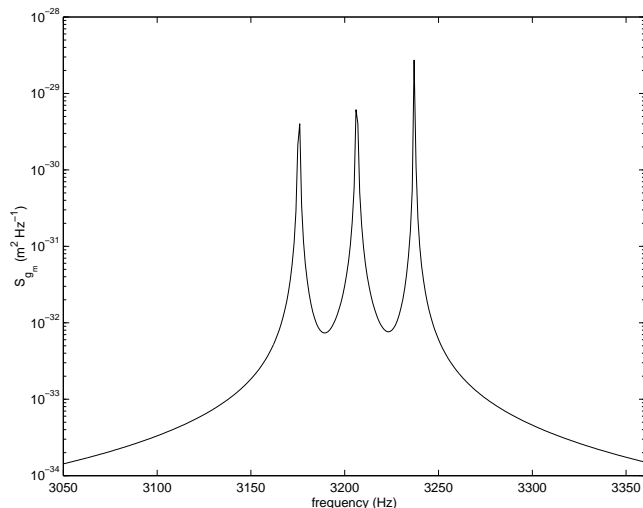


FIG. 13: Spectral density of the contributions of the Langevin forces to the mode channels.

with  $S^{\tilde{F}_m^S} \equiv \tilde{F}_m^S * \tilde{F}_m^S$  and  $S^{\tilde{F}_{ji}^N} \equiv \tilde{F}_{ji}^N * \tilde{F}_{ji}^N$ . As an example one can calculate the noise contribution from Langevin forces, which have spectral densities well known and given by

$$S^{FL_i} = \frac{4k_B T m_i \omega}{Q_i}, \quad (43)$$

where  $k_B = 1.38 \times 10^{-23}$  J/K is Boltzman's constant,  $T$  is physical temperature of the system, and  $m_i$  and  $Q_i$  are respectively the physical mass and the mechanical quality factor of the body  $i$ .

From the calculation of the of the spectral density  $S_m^g(\omega)$ , assuming no incident GW signal, we found that the contributions to each normal mode seem to have the same spectral densities, but with slightly different values, since each one of them receives different contributions from each of the resonators (See Figure VII). These contributions are small compared to those originated from the sphere since the resonators' masses are much smaller than the sphere's mass ( $m_s/Q_s \sim 34m_{R1}/Q_{R1} \sim 5.7 \times 10^3 m_{R2}/Q_{R2}$ , using the adopted values). The agreement among the values of  $S_m^g(\omega)$  is also a consequence of the fact that we have initially assumed that all the modes have the same transfer function,  $\xi(\omega)$ . The use of different transfer functions for each mode  $m$  may help the understanding on how asymmetries on the real sphere should affect the individual responses of the modes to GWs [16].

The GW effective force (eq. 14) that acts on the sphere (in the frequency domain) has spectral density

$$S_m^{\mathcal{F}_{GW}}(\omega) = \left( \frac{1}{2} \omega^2 m_S \chi R \right)^2 S_m^{\tilde{h}}(\omega). \quad (44)$$

The sensitivity curve for mode  $m$  is given through

$$\tilde{h}_m(\omega) = \sqrt{\frac{1}{\left( \frac{1}{2} \omega^2 m_S \chi R \right)^2 |\xi_m(\omega)|^2} S_m^g(\omega)}. \quad (45)$$

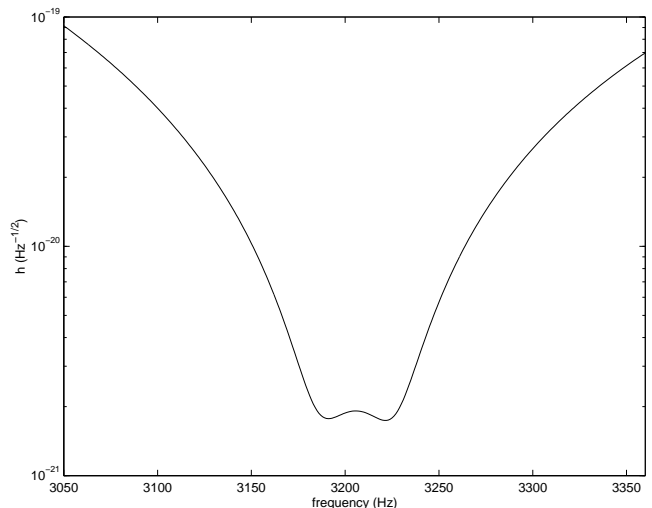


FIG. 14: Sensitivity curve for the mode channels.

Figure VII shows the sensitivity curves for the five quadrupolar normal modes of the sphere. We obtained this curve assuming that no signal was present and that only the usual noises in this kind of detector (Brownian noise, serial noise, back-action noise and electronic phase and amplitude noises) were disturbing the antenna.

From reasonable estimates of the spectral densities of the noise sources it is possible to determine their contributions to the mode channels and, consequently, the values of  $\tilde{h}_m(\omega)$ , which allow for the location of the GW source in the sky, as well as the determination of the polarization amplitudes of the GW.

## VIII. CONCLUSION

In this work we presented a model that describes the response to a gravitational wave of the spherical GW detector SCHENBERG coupled to six one-dimensional two-mode transducers .

The analytical expressions obtained as solutions of the equation of motion for the system are in good agreement with the numerical solutions.

We found an expression (Equation 42) which allows for estimates of the contributions of the noises to the mode channels. Such an expression is very much needed for a more realistic modelling of the SCHENBERG detector.

## APPENDIX A: EINGENVECTOR SOLUTIONS

In order to determine the values of the constants  $n_k, c_k, d_k, n_{1\pm}$  and  $d_{1\pm}$  we imposed that  $\underline{\underline{U}}$  must be Hermitian and

$$\underline{\underline{MU}} = \underline{\underline{UD}}. \quad (A1)$$

We separate the two groups of eigenvectors ( $\underline{U}_{1\pm}$  and  $\underline{U}_k$ ) and solve equation A1 using

$$\underline{\underline{M}}\underline{U}_{1\pm} = \underline{U}_{1\pm}D_{1\pm}, \quad (\text{A2})$$

$$\underline{\underline{M}}\underline{U}_k = \underline{U}_k D_k, \quad (\text{A3})$$

where  $D_{1\pm} \equiv \lambda_{1\pm}$  and  $D_k \equiv \lambda_k$  are the eigenvalues of eigenvectors  $\underline{U}_{1\pm}$  and  $\underline{U}_k$  respectively. So, by using the properties of the  $\underline{B}$  matrix we obtain the following expressions for the constants:

$$n_{1\pm}^2 = \frac{1}{1 + \frac{3}{2\pi}(1 + d_{1\pm}^2)}, \quad (\text{A4})$$

$$d_{1\pm} = -\frac{1}{2}(a \pm \sqrt{a^2 + 4}), \quad (\text{A5})$$

$$n_k^2 = \frac{1}{1 + \frac{3}{2\pi}(c_k^2 + d_k^2)}, \quad (\text{A6})$$

$$d_k = \frac{3}{2\pi} \frac{b}{a} \left( c_k^2 + bc_k - \frac{2\pi}{3} \right), \quad (\text{A7})$$

$$c_2 = \frac{s_3^2 + 4x^2 - 2xs_3 - 2y}{6s_3}, \quad (\text{A8})$$

$$c_{3,4} = \frac{4(-1 \mp i\sqrt{3})x^2 + (-1 \pm i\sqrt{3})s_3^2 - 4xs_3}{12s_3} + \frac{1 \pm i\sqrt{3}}{s_3}, \quad (\text{A9})$$

where

$$i = \sqrt{-1}, \quad (\text{A10})$$

$$s_3 = (s_1 + 12\sqrt{s_2})^{1/3}, \quad (\text{A11})$$

$$s_1 = -8sx^3 + 36xy - 108z, \quad (\text{A12})$$

$$12y^3 + 12x^3z - 3x^2y^2 + 81z^2 - 54xyz, \quad (\text{A13})$$

$$x = \frac{2\pi}{3} \left( \frac{a^2}{b} + \frac{3}{2\pi}b \right), \quad (\text{A14})$$

$$y = \frac{2\pi}{3} \left[ \frac{a^2}{b^2} \left( b^2 - \frac{2\pi}{3} \right) - 1 \right] \quad (\text{A15})$$

$$z = -\frac{4\pi^2}{9} \frac{a^2}{b}. \quad (\text{A16})$$

Those imply that

$$\lambda_{1\pm} = 1 - ad_{1\pm} \quad (\text{A17})$$

and

$$\lambda_k = 1 - \frac{3}{2\pi}b^2c_k. \quad (\text{A18})$$

Although  $c_{3,4}$  ( $c_k$  with  $k = 3, 4$ ) has imaginary terms its value is real, which satisfies Hermitian condition for eigenvectors.

We also can define the quantities

$$\eta_{1\pm} = \eta_{1\pm}(\omega) = \frac{n_{1\pm}}{\omega_{1\pm}^2 - \omega^2} \quad (\text{A19})$$

and

$$\eta_k = \eta_k(\omega) = \frac{n_k}{\omega_k^2 - \omega^2}. \quad (\text{A20})$$

These quantities help us to write an analytic expression for the mode channel outputs.

## ACKNOWLEDGMENTS

This work was supported by **FAPESP** (under grant numbers 1998/13468-9, 2001/14527-3 and 2003/02912-5), **CNPq** (under grant number 300619/92-8) and **MCT/INPE**.

- 
- [1] A. Einstein, *Naherungsweise Integration der Field Gleichungen der Gravitation* (Sitzungsberichte der Koniglich Preussischen Akad. der Wissenschaften, 1916), pp. 688–696.  
 [2] J. A. Weber, Phys. Rev. **177**, 306 (1960).  
 [3] J. H. Taylor, Rev. of Modern Phys. **66**, 711 (1994).

- [4] R. L. Forward, Gen. Relat. and Grav. **2**, 149 (1971).  
 [5] N. Ashby and J. Dreitlein, Phys. Rev. D **12**, 336 (1975).  
 [6] R. V. Wagoner and H. J. Paik, *Proceedings of the Acad. Nazionale dei Lincei Intern. Sympos. on Experim. Gravitation* (World Scientific, 1976), pp. 257–266.  
 [7] W. Johnson and S. M. Merkowitz, Phys. Rev. Letters **70**,

- 2367 (1993).
- [8] N. S. Magalhaes, O. D. Aguiar, W. W. Johnson, and C. Frajuca, *Gen. Relat. Grav.* **29**, 1509 (1997).
  - [9] M. Bianchi, E. Coccia, C. N. Colacino, V. Fafone, and F. Fucito, *Class. Quantum Grav.* **13**, 2865 (1996).
  - [10] S. M. Merkowitz and W. W. Johnson, *Phys. Rev. D* **56**, 7513 (1997).
  - [11] G. B. Arfken and H. J. Weber, *Mathematical methods for physicists* (HAP, 2000).
  - [12] G. M. Harry, T. R. Stevenson, and H. J. Paik, *Phys. Rev. D* **54**, 2409 (1996).
  - [13] S. M. Merkowitz, *Phys. Rev. D* **58**, 062002 (1998).
  - [14] R. B. Scott, *Cryogenic Engineering* (Van Nostrand, 1963).
  - [15] J. P. Richard, in *Proceedings of 2nd Marcel Grossman Meeting* (1982), pp. 324–343.
  - [16] T. R. Stevenson, Tech. Rep., University of Maryland (1996).